JACS
JOURNAL OF THE AMERICAN CHEMICAL SOCIETY

Communication

pubs.acs.org/JACS

Preparation and Exceptional Lithium Anodic Performance of Porous Carbon-Coated ZnO Quantum Dots Derived from a Metal–Organic Framework

Seung Jae Yang,[†] Seunghoon Nam,[‡] Taehoon Kim,[†] Ji Hyuk Im,[†] Haesol Jung,[†] Jong Hun Kang,[†] Sungun Wi,[‡] Byungwoo Park,[‡] and Chong Rae Park*[,†]

[†]Carbon Nanomaterials Design Laboratory, Global Research Laboratory, Research Institute of Advanced Materials, and Department of Materials Science and Engineering, Seoul National University, Seoul 151-744, Korea

[‡]WCU Hybrid Materials Program, Department of Materials Science and Engineering, Research Institute of Advanced Materials, Seoul National University, Seoul 151-744, Korea

Supporting Information

ABSTRACT: Hierarchically porous carbon-coated ZnO quantum dots (QDs) (~3.5 nm) were synthesized by a one-step controlled pyrolysis of the metal–organic framework IRMOF-1. We have demonstrated a scalable and facile synthesis of carbon-coated ZnO QDs without agglomeration by structural reorganization. This unique microstructure exhibits outstanding electrochemical performance (capacity, cyclability, and rate capability) when evaluated as an anode material for lithium ion batteries.

Lithium ion batteries (LIBs), a fast-developing technology area in electric energy storage, are a promising power source for a wide range of portable electronic devices.[1,2] A variety of materials may be used in LIBs. As an example, metal oxides can potentially be substituted for graphite (~370 mA h g^{-1}) in current platforms to meet the demand for high capacities.[1−3] Most metal oxides undergo an undesirable large volume change that leads to a dramatic falloff in capacity during cycling. Several methods have been developed to overcome this problem, including the fabrication of nanostructured electrodes, such as nanoparticles, nanowires, or nanotubes, or the preparation of hybrid composites with an inactive matrix, such as carbon, that mechanically buffers against volume changes.[1−6]

Metal–organic frameworks (MOFs) represent an emerging class of materials that have attracted extensive research interest because of their tunable porosities and versatile functionalities.[7] Numerous applications have been investigated, including gas storage and separation, catalysis, sensing, and gas chromatography.[8−10] In recent years, several theoretical and experimental approaches have indicated that some MOFs behave as semiconductors in metal oxide quantum dot (QD) configurations.[11] Such MOFs exhibit photocatalytic activities and photoluminescence (PL) that result from their hybrid structures involving periodically dispersed metal oxide clusters separated by organic spacers. The properties of the hybrid structures have motivated the development of facile preparations of well-dispersed metal oxide QDs embedded in porous carbon matrices comprising MOFs (Figure 1) as well as studies of anode LIB materials with minimal volume changes during cycling.

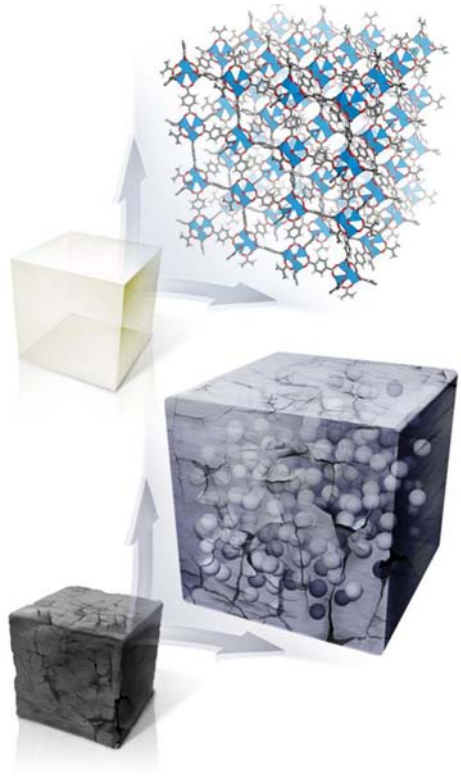

Figure 1. Schematic diagrams of IRMOF-1 (top) and IRMOF-1 after controlled pyrolysis to produce carbon-coated ZnO QDs without agglomeration (bottom). The ZnO QDs are covered with a thin amorphous carbon layer that acts as a buffer layer to confine the QDs during the charging and discharging steps.

In this work, we examined isoreticular MOF-1 (IRMOF-1, conventionally denoted as MOF-5; Figure S1 in the Supporting Information) as a case study because it is amenable to mass production, it has high crystallinity, and its purity can be excellent.[12] Although preparations of porous Fe_2O_3 bulk materials from Fe-based MOFs[13,14] have recently been reported,

Received: November 26, 2012
Published: May 7, 2013

   dx.doi.org/10.1021/ja311550t | J. Am. Chem. Soc. 2013, 135, 7394−7397

those studies focused only on the metallic product after removal of the organic constituent of the MOF. Unlike the previous reports, we have developed a novel and facile approach to the synthesis of zinc oxide (ZnO) QDs (~3.5 nm) without intrinsic defects or agglomeration embedded in hierarchically porous carbon matrices derived from IRMOF-1. The tailor-fit microstructures enabled the display of exceptionally high Li storage performances. Thus, the proposed method provides new effective ways to fabricate high-performance anode materials based on a metal oxide@porous carbon matrix.

The structural reorganization of the MOF to ZnO QDs@porous carbon, synthesized via a controlled pyrolysis reaction to obtain the initial state of the transformation (Figure S2), was investigated by scanning electron microscopy (SEM) and transmission electron microscopy (TEM). The samples are designated by the heat treatment temperature (in °C) followed by the atmospheric conditions (e.g., "550N" denotes a sample heated at 550 °C under an inert atmosphere). SEM micrographs (Figure 2a,b) indicated that 550N retained the pristine cubic

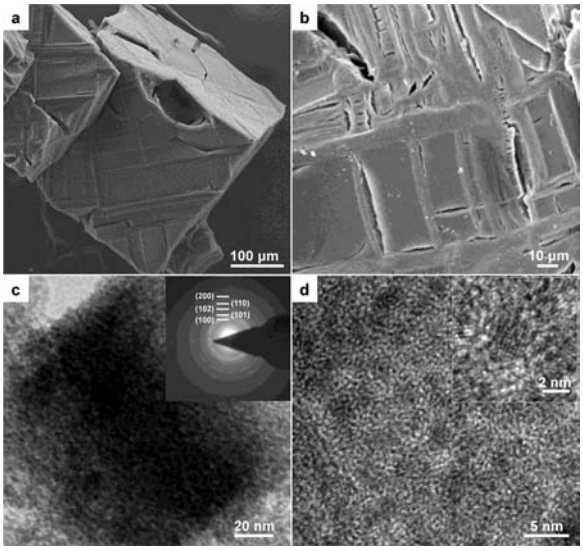

Figure 2. ZnO QDs@porous carbon (550N) obtained from IRMOF-1: (a, b) SEM images; (c) TEM image (inset: SAED pattern); (d) high-resolution TEM image (inset: enlarged view).

morphology of the as-prepared IRMOF-1 even after high-temperature heating.[15,16] Black microparticles were observed (Figure S3), with cracked surfaces that developed during decomposition of the organic species.[12,16] TEM images revealed that the cubic microparticles consisted of ZnO QDs and amorphous carbon. The selected-area electron diffraction (SAED) pattern (Figure 2c inset) displayed a typical hexagonal wurtzite crystal structure of ZnO, indicating that the carbon obtained was nearly amorphous and lacked long-range order. Figures 2d and S4 clearly confirmed that the highly crystalline ZnO QDs were well-dispersed, not agglomerated, and nearly monodisperse, with a mean particle size of 3 ± 1 nm in the amorphous carbon matrix.

Figure 3a presents an X-ray diffraction (XRD) pattern for 550N with Bragg peaks corresponding to ZnO, consistent with the SAED patterns. The corresponding ZnO peaks exhibited line broadening due to the small size of the obtained ZnO particles. The measured size of the ZnO particles as determined using the Scherrer formula (Figure S5) was approximately 3.5 nm, in good agreement with the TEM results.[17] PL spectroscopy was used to

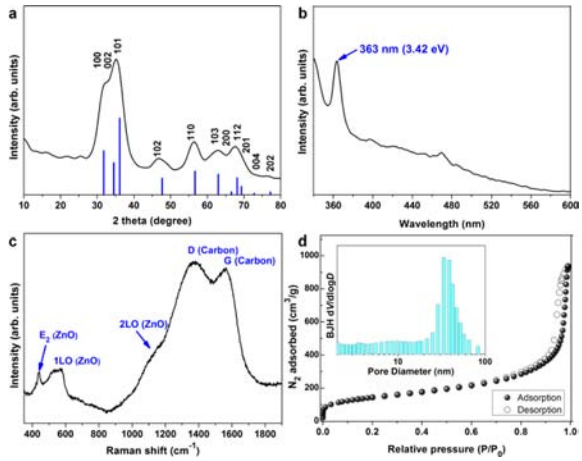

Figure 3. (a) XRD pattern, (b) PL spectrum, (c) Raman spectrum, and (d) nitrogen adsorption isotherm at 77 K for the 550N sample. The inset in (d) is the pore size distribution calculated using the BJH equation.

characterize the atomic defects and crystalline size of the ZnO. In the PL spectrum (Figure 3b), the predominant PL emission peak occurred at 363 nm (3.42 eV). This peak is blue-shifted compared with the excitonic emission peak corresponding to a typical band gap of bulk ZnO (3.36 eV).[17,18] The shift in the emission peak was ascribed to a quantum-confinement-induced energy gap enhancement, further emphasizing the quantum size of the resultant ZnO. Another notable feature of this spectrum is the lack of a low-energy blue-green emission band due to the surface defects associated with oxygen vacancies or interstitial zinc sites.[16−18] Combined with the X-ray photoemission spectroscopy (XPS) analysis of 550N (Figure S6), this result indicated that the ZnO QDs were high in quality.

As revealed by TEM imaging, the Raman spectrum of the 550N sample (Figure 3c) confirmed the coexistence of ZnO QDs and amorphous carbon. The 550N sample displayed two distinct bands at 1320 and 1590 cm^{-1} assigned to the typical D and G bands of amorphous carbon, respectively, and three different bands associated with the ZnO QDs.[16,18,19] The E_2 phonon frequency occurs at 436 cm^{-1} for ZnO QDs with sizes of less than 10 nm, which is red-shifted from 475 cm^{-1} for bulk ZnO particles.[18] Combined with the PL and XRD results, the E_2 band of 550N strongly supported the formation of ZnO QDs. The textural characteristics of the product were quantified by measuring the nitrogen adsorption isotherm (Figure 3d) at 77 K. The specific surface area (SSA) calculated using the Brunauer−Emmett−Teller (BET) equation and the total pore volume at P/P_0 = 0.98 were 513 $m^2\ g^{-1}$ and 1.27 $cm^3\ g^{-1}$, respectively. The pore size distribution calculated using the Barrett−Joyner−Halenda (BJH) equation (Figure 3d inset) revealed a mesoporosity of the resultant material centered at 35 nm. Combined with the observation of a considerable increase of nitrogen adsorption at low pressure, this material exhibited a hierarchical pore system consisted of micro- and mesopores. In view of the quantity of amorphous carbon in the 550N sample [32 wt % as determined by thermogravimetric analysis (TGA); Figure S7], a BET SSA of 513 $m^2\ g^{-1}$ is remarkably high compared with the values reported for metal oxide@porous carbon composites.[3,6] This high SSA, coupled with the TEM, XRD, PL, and Raman results, was attributable to the formation of unagglomerated, quantum-sized ZnO and porous carbon hybrid particles.

dx.doi.org/10.1021/ja311550t | J. Am. Chem. Soc. 2013, 135, 7394−7397

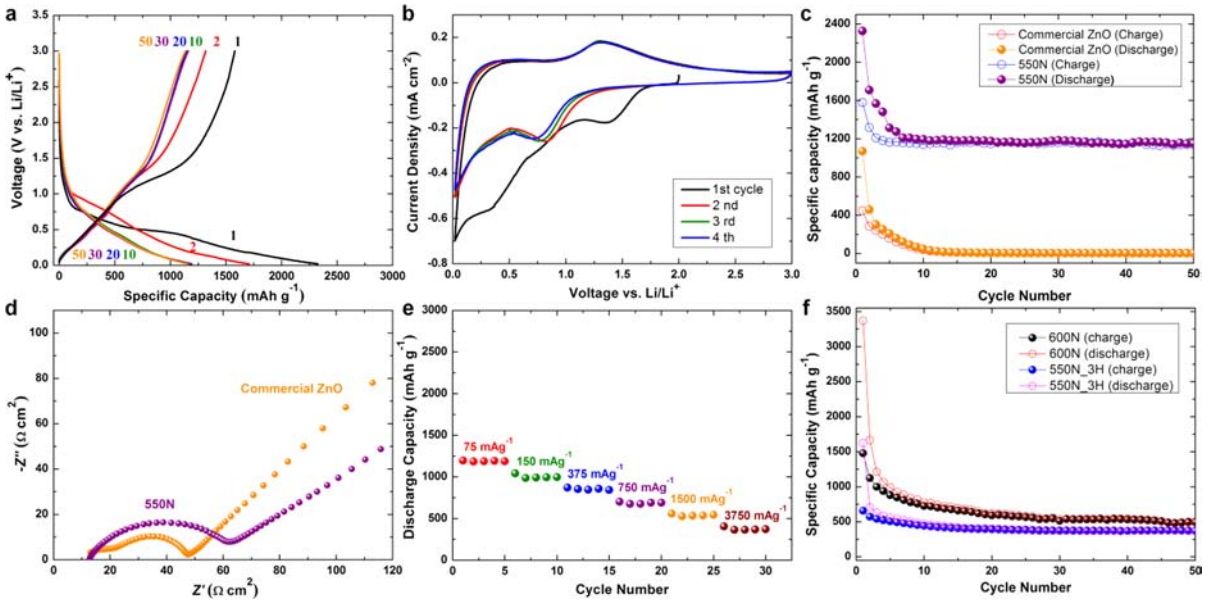

Figure 4. (a) Voltage profile of 550N. The cell was tested for 50 cycles between 20 mV and 3.0 V under a current density of 75 mA g^{-1}. (b) Cyclic voltammetry measurements on 550N during the first four cycles. The voltage range was 20 mV to 3.0 V at a scan rate of 0.1 mV s^{-1}. The initial point corresponded to the open-circuit voltage of the cell. (c) Cycle-life performances of 550N and the commercial ZnO counterpart (75 mA g^{-1}). (d) Nyquist plots for 550N and the commercial ZnO powder after three cycles under an applied voltage of 0.256 V. (e) Discharge capacity of 550N at various current densities. The cells were cycled 20 times at a current density of 75 mA g^{-1} prior to variation of the current density from 75 to 3750 mA g^{-1}. (f) Cycle-life performances of 600N and 550N_3H at a current density of 75 mA g^{-1}.

The formation of ZnO QDs@porous carbon was investigated in detail by carrying out the pyrolysis of MOFs under various conditions (Figures S8−S11). At high target temperatures, the QDs readily ripened, and the resultant particles were estimated to be ∼20 nm in size (XRD results) without a uniform shape (TEM image). Aside from the target temperature, the duration of heating at 550 °C and the heating rate played important roles in the evolution of the nanostructures. Irregular ripening of the ZnO QDs occurred, as observed at higher target temperatures. The high surface energies of the very small particles may have accelerated the ripening, even under slightly different conditions. The pyrolysis conditions led to a reduction in ZnO while simultaneously inducing surface defects. The PL characteristics of the materials were consistent with the observation of a green emission band corresponding to O defects on the obtained ZnO crystals (Figure S12).[15,16,18,20]

The galvanostatic charge/discharge curve for 550N is presented in Figure 4a. The plateau in the first cycle indicated a three-phase equilibrium region in the Zn−Li−O system (ZnO−Li_2O−Zn). The large initial capacity (∼2300 mA h g^{-1}) can be understood on the basis of the reduction of ZnO to give Zn plus the formation of a solid−electrolyte interphase (SEI) layer on the surface of the ZnO QDs@porous carbon. These reactions were supported by the cyclic voltammetry measurements (Figure 4b), in which the first scan curve differed significantly from subsequent cycles. The initial capacity was lost in a continuous way during the first few cycles, after which the cycle-life performance of 550N stabilized. The initial loss of capacity arose mainly from the incomplete conversion reaction and irreversible lithium loss due to the formation of the SEI layer.[21] This leads to poor Coulombic efficiency, and such an irreversible capacity is deleterious to practical applications. Intensive work should be expended in the future to improve the first Coulombic efficiency. The capacity after the seventh cycle, however, tended to saturate with a discharge capacity of 1150 mA h g^{-1}. It should be noted that some of the reversible capacity (∼107 mA h g^{-1}) originated from the Super P carbon black, considering that it stores lithium ion (Figure S13) and was 20 wt % of the whole electrode. This performance far surpasses that of any other material based on ZnO.[22] The cycle-life performance of 550N is shown in Figure 4c along with that of commercial ZnO nanopowder (Aldrich; for its XRD and nitrogen adsorption isotherm, see Figure S14) measured for comparison purposes. The cells prepared with the commercial ZnO nanopowder died only after 10 cycles, as reported earlier.[23] It should be noted that the capacity here is that of the ZnO QDs plus that of the amorphous carbon, and the C rate was calculated on the basis of the theoretical capacity considering the relative amounts of ZnO and amorphous carbon: 981 (ZnO) × 0.68 + 470 (amorphous carbon; Figure S15) × 0.32 = 817 mA h g^{-1} for 550N. The capacity of amorphous carbon only is displayed in Figure S15.

Interestingly, the measured capacity exceeded the theoretically predicted capacity, and the cyclability was exceptional compared with the reported values.[22−24] The origin of the outstanding performance is that each ZnO QD was coated with amorphous carbon in the highly long-range-ordered structure of the MOF precursor.[7] Complete encapsulation of nanoparticles is not ensured in conventional amorphous carbon-coated ZnO, whereas the framework yielded a relatively uniform well-defined coating layer. The carbon coating layer effectively prevented volume expansion during consecutive alloying−dealloying processes. The beneficial buffer effect was qualitatively measured using Nyquist plots for 550N and the commercial ZnO nanopowder (Figure 4d). The impedance associated with the charge-transfer resistance in 550N exceeded that of the commercial ZnO nanopowder. The amorphous carbon layer synthesized at a relatively low temperature (550 °C) may not have contributed significantly to the conductivity as a result of the insufficient thermal treatment and nongraphitizable precursor, leading us to conclude that the electrochemical

dx.doi.org/10.1021/ja311550t | J. Am. Chem. Soc. 2013, 135, 7394−7397

performance of ZnO depended more on buffering of the volume expansion.[25,26] The commercial ZnO nanopowder exhibited a circle in the Nyquist plot due to the SEI layer (Figure 4d), whereas 550N exhibited only a single circle associated with the charge-transfer resistance. The amorphous carbon may have reduced the undesirable growth of the SEI layer.[27] Consequently, the circle associated with the SEI layer in the Nyquist plot of 550N was insignificant. Furthermore, the large surface area of such small-sized QDs (~3.5 nm) might contribute to extra charge storage, which was found to be reversible during cycling, leading to a capacity exceeding 982 mA h g^{-1} ($C_{theoretical}$ of ZnO).[28] It is presumed that the surface of the ZnO QDs is greatly exposed to the Li^+ environment since each QD is separated by amorphous carbon. Therefore, several phenomena, such as interfacial charge storage via weakly bound Li at the surface of ZnO QDs, reactions with the electrolyte, and charge separation at the SEI layer could possibly occur, to which the extra capacity is attributed.[29,30] On the contrary, the carbon-coated nanoparticles reported to date became more or less aggregated during battery cycling, and therefore, the contribution of capacity from alternative ways of Li storage seemed negligible. The ZnO QD size benefited the rate of Li ion diffusion, as reflected in the rate capability results (Figure 4e). The above discussion reveals that the ZnO particle size increased dramatically, and the particles included many internal defects, leading to poorer electrochemical properties than were observed in the 550N sample. The cycle-life performances of the 600N and 550N_3H samples, both of which displayed large particle sizes, are illustrated in Figure 4f. The higher initial irreversible capacity of 600N compared with that of the 550N might be due to the severe SEI formation on the surface of the porous carbon in 600N.[31−33] Both the crystal size and perfectness of the ZnO particles made important contributions to the enhanced electrochemical performance.

In summary, a controlled pyrolysis of MOFs for the synthesis of porous carbon-coated ZnO QDs without agglomeration has been demonstrated. The materials exhibited promising Li storage properties and high specific charge capacities (~1200 mA h g^{-1} at 75 mA g^{-1}). The capacity was estimated on the basis of the total composite weight, the stable cyclability (~50 cycles with nearly 100% capacity retention), and the good performance rate (~400 mA h g^{-1} at 3750 mA g^{-1}). The very first Coulombic efficiency that arises from the high initial discharge capacity is significantly low, and this should be resolved in the future from a practical point of view. Nonetheless, the novel and facile synthesis introduced here provides insight into the ZnO system, which has not been extensively examined to date for use as an LIB anode. This concept may potentially be expanded to other high-capacity metal oxide anode material systems that undergo a large volume expansion during an electrochemical reaction.

■ ASSOCIATED CONTENT

Supporting Information

Experimental section and additional data. This material is available free of charge via the Internet at http://pubs.acs.org.

■ AUTHOR INFORMATION

Corresponding Author

crpark@snu.ac.kr

Notes

The authors declare no competing financial interest.

■ ACKNOWLEDGMENTS

This work was supported by National Research Foundation of Korea (NRF) Grants funded by the Korean Government (MEST) (2010-0029244 and 2012-0000580).

■ REFERENCES

(1) Bruce, P. G.; Scrosati, B.; Tarascon, J.-M. *Angew. Chem., Int. Ed.* **2008**, *47*, 2930.
(2) Scrosati, B.; Hassoun, J.; Sun, Y.-K. *Energy Environ. Sci.* **2011**, *4*, 3287.
(3) Wu, Z.-S.; Zhou, G.; Yin, L.-C.; Ren, W.; Li, F.; Cheng, H.-M. *Nano Energy* **2012**, *1*, 107.
(4) Myung, S.-T.; Takahashi, N.; Komaba, S.; Yoon, C. S.; Sun, Y.-K.; Amine, K.; Yashiro, H. *Adv. Funct. Mater.* **2011**, *21*, 3231.
(5) Lee, J.-I.; Lee, K. T.; Cho, J.; Kim, J.; Choi, N.-S.; Park, S. *Angew. Chem., Int. Ed.* **2012**, *51*, 2767.
(6) Lee, K. T.; Cho, J. *Nano Today* **2011**, *6*, 28.
(7) Farrusseng, D.; Aguado, S.; Pinel, C. *Angew. Chem., Int. Ed.* **2009**, *48*, 7502.
(8) Lee, C. Y.; Bae, Y.-S.; Jeong, N. C.; Farha, O. K.; Sarjeant, A. A.; Stern, C. L.; Nickias, P.; Snurr, R. Q.; Hupp, J. T.; Nguyen, S. T. *J. Am. Chem. Soc.* **2011**, *133*, 5228.
(9) Lan, Y.-Q.; Jiang, H.-L.; Li, S.-L.; Xu, Q. *Adv. Mater.* **2011**, *23*, 5015.
(10) Gu, Z.-Y.; Yan, X.-P. *Angew. Chem., Int. Ed.* **2010**, *49*, 1477.
(11) Bordiga, S.; Lamberti, C.; Ricchiardi, G.; Regli, L.; Bonino, F.; Damin, A.; Lillerud, K. P.; Bjorgen, M.; Zecchina, A. *Chem. Commun.* **2004**, 2300.
(12) Yang, S. J.; Park, C. R. *Adv. Mater.* **2012**, *24*, 4010.
(13) Zhang, L.; Wu, H. B.; Madhavi, S.; Hng, H. H.; Lou, X. W. *J. Am. Chem. Soc.* **2012**, *134*, 17388.
(14) Xu, X.; Cao, R.; Jeong, S.; Cho, J. *Nano Lett.* **2012**, *12*, 4988.
(15) Liu, B.; Shioyama, H.; Akita, T.; Xu, Q. *J. Am. Chem. Soc.* **2008**, *130*, 5390.
(16) Yang, S. J.; Kim, T.; Im, J. H.; Kim, Y. S.; Lee, K.; Jung, H.; Park, C. R. *Chem. Mater.* **2012**, *24*, 464.
(17) Feng, P. L.; Perry, J. J., IV; Nikodemski, S.; Jacobs, B. W.; Meek, S. T.; Allendorf, M. D. *J. Am. Chem. Soc.* **2010**, *132*, 15487.
(18) Son, D. I.; Kwon, B. W.; Park, D. H.; Seo, W.-S.; Yi, Y.; Angadi, B.; Lee, C.-L.; Choi, W. K. *Nat. Nanotechnol.* **2012**, *7*, 465.
(19) Hu, Y.-S.; Demir-Cakan, R.; Titirici, M.-M.; Müller, J.-O.; Schlögl, R.; Antonietti, M.; Maier, J. *Angew. Chem., Int. Ed.* **2008**, *47*, 1645.
(20) Vanheusden, K.; Warren, W. L.; Seager, C. H.; Tallant, D. R.; Voigt, J. A.; Gnade, B. E. *J. Appl. Phys.* **1996**, *79*, 7983.
(21) Wu, Z.-S.; Ren, W.; Wen, L.; Gao, L.; Zhao, J.; Chen, Z.; Zhou, G.; Li, F.; Cheng, H.-M. *ACS Nano* **2010**, *4*, 3187.
(22) Ahmad, M.; Yingying, S.; Nisar, A.; Sun, H.; Shen, W.; Wei, M.; Zhu, J. *J. Mater. Chem.* **2011**, *21*, 7723.
(23) Huang, X. H.; Xia, X. H.; Yuan, Y. F.; Zhou, F. *Electrochim. Acta* **2011**, *56*, 4960.
(24) Wang, H.; Pan, Q.; Cheng, Y.; Zhao, J.; Yin, G. *Electrochim. Acta* **2009**, *54*, 2851.
(25) Kushima, A.; Liu, X. H.; Zhu, G.; Wang, Z. L.; Huang, J. Y.; Li, J. *Nano Lett.* **2011**, *11*, 4535.
(26) Nam, S.; Kim, S.; Wi, S.; Choi, H.; Byun, S.; Choi, S.-M.; Yoo, S.-I.; Lee, K. T.; Park, B. *J. Power Sources* **2012**, *211*, 154.
(27) Yoo, J.-K.; Kim, J.; Jung, Y. S.; Kang, K. *Adv. Mater.* **2012**, *24*, 5452.
(28) Qie, L.; Chen, W.-M.; Wang, Z.-H.; Shao, Q.-G.; Li, X.; Yuan, L.-X.; Hu, X.-L.; Zhang, W.-X.; Huang, Y.-H. *Adv. Mater.* **2012**, *24*, 2047.
(29) Jamnik, J.; Maier, J. *Phys. Chem. Chem. Phys.* **2003**, *5*, 5215.
(30) Wu, Y.; Wei, Y.; Wang, J.; Jiang, K.; Fan, S. *Nano Lett.* **2013**, *13*, 818.
(31) Hu, Y. S.; Adelhelm, P.; Smarsly, B. M.; Hore, S.; Antonietti, M.; Maier, J. *Adv. Funct. Mater.* **2007**, *17*, 1873.
(32) Guo, B.; Wang, X.; Fulvio, P. F.; Chi, M.; Mahurin, S. M.; Sun, X.-G.; Dai, S. *Adv. Mater.* **2011**, *23*, 4661.
(33) Fang, Y.; Lv, Y.; Che, R.; Wu, H.; Zhang, X.; Gu, D.; Zheng, G.; Zhao, D. *J. Am. Chem. Soc.* **2013**, *135*, 1524.